PUBLISHED BY IOP PUBLISHING FOR SISSA
RECEIVED: *March 14, 2011*
ACCEPTED: *May 18, 2011*
PUBLISHED: *May 31, 2011*

Performance evaluation of a PET detector consisting of an LYSO array coupled to a 4×4 array of large-size GAPD for MR compatible imaging

Key Jo Hong,[a,b] **Yong Choi,**[a,b,1] **Jihoon Kang,**[a,b] **Wei Hu,**[a,b] **Jin Ho Jung,**[a,b] **Byung Jun Min,**[a,b] **Yong Hyun Chung**[c] **and Carl Jackson**[d]

[a] *Department of Electronic Engineering, Sogang University, 1 Shinsu-Dong, Mapo-Gu, Seoul 121-742, Republic of Korea*
[b] *Sungkyunkwan University School of Medicine, 50 Ilwon-Dong, Gangnam-Gu, Seoul 135-710, Republic of Korea*
[c] *Department of Radiological Science, Yonsei University, College of Health Science, 234 Meaji, Heungup Wonju, Kangwon-Do, 220-710, Republic of Korea*
[d] *SensL, Blackrock, Cork, Ireland*

E-mail: ychoi@sogang.ac.kr

ABSTRACT: We examined a PET detector consisting of an LYSO array coupled to a 4 × 4 array of large-size Geiger-mode avalanche photodiode (GAPD). The GAPD coupled to 3 mm × 3 mm × 20 mm LYSO pixel crystal has been investigated for possible use as an MR-compatible PET photosensor. Primary characteristics of a PET detector, such as energy resolution and coincidence timing resolution were measured. Gain variation, count uniformity, and count estimation error of 4 × 4 array of LYSO-GAPD were measured to evaluate the performance parameters relevant for PET imaging. The energy resolution and coincidence timing resolution with 511 keV gamma rays were 18.5 ± 0.7% and 1.6 ns, respectively. The gain variation, count uniformity for all 16 channels were 1.3:1 and 1.3:1, respectively. The count estimation error between adjacent channels measured with an LYSO connected to a GAPD pixel was negligible (0.24 ± 0.04%). Long-term stability results show that there was no significant change in the photopeak position, energy resolution and count rate for 20 days. Cable lengths up to 300 cm, used between the GAPD and preamplifier, did not affect photopeak position and energy resolution. The performance of the LYSO-GAPD detector inside the MRI exhibited no significant change compared to that measured outside the MRI. The MR images acquired with and without the operating LYSO-GAPD detector located on top of the RF coil showed no considerable degradation in image quality. These results demonstrate the feasibility of using the LYSO-GAPD detector as PET photosensors, which could be used for MR compatible PET development.

KEYWORDS: Photon detectors for UV, visible and IR photons (solid-state) (PIN diodes, APDs, Si-PMTs, G-APDs, CCDs, EBCCDs, EMCCDs etc); Gamma camera, SPECT, PET PET/CT, coronary CT angiography (CTA); Multi-modality systems

[1] Corresponding author. Telephone number: +82-2-705-8910, Fax: +82-2-706-4216.

doi:10.1088/1748-0221/6/05/P05012

2011 JINST 6 P05012

Contents

2011 JINST 6 P05012

1 Introduction

Recently, positron emission tomography (PET) has evolved into multi-modality imaging systems obtaining quantitative functional information with accurate anatomical detail [1–3]. PET combined with computed tomography (CT) has been widely utilized in clinical and preclinical studies. As a subsequent advancement, a combination of PET and magnetic resonance imaging (MRI) has been proposed, not only because of the absence of ionizing radiation in MRI but also for its excellent soft-tissue contrast and its capability to perform diffusion imaging, magnetic resonance spectroscopy (MRS) and functional MRI (fMRI) [4–6]. Thus, current developments on PET detector technology are focusing on the combination of PET and MRI to obtain simultaneous images from both modalities [5, 7–11].

Simultaneous PET and MRI acquisition requires a highly demanding detector design without degrading the original optimum performance of either [6]. One of the major problems of combining PET and MRI is the fact that the performance of the photomultiplier tubes (PMTs) used in conventional PET detectors is extremely sensitive to the magnetic field required for MRI. To overcome this problem, long optical fibers were employed to transfer the light signals from scintillation crystals located inside the MRI system to PMTs located at a distance far enough to ensure normal

function [8,9,11-15]. Use of optical fibers, however, can degrade the overall PET performance caused by the light transmission via optical fibers over several meters, resulting in reduced timing resolution, energy resolution, and crystal decoding accuracy [9].

Several studies have reported on the fabrication of the combined PET and MRI based on avalanche photodiodes (APDs) instead of the PMTs in PET detectors [7, 9, 16–19]. APDs are considered advantageous over PMTs due to their compactness, high quantum efficiency and insensitivity to high magnetic fields [20]. However, the low internal gain (in the range of 100–100,000) of APDs requires the use of sophisticated, low noise pre-amplifiers, which furthermore will require stringent electro-magnetic interference (EMI) shielding inside the limited field-of-view (FOV) of the MRI system [6].

In recent years, Geiger-mode avalanche photodiodes (GAPDs) have attracted interest for their use as scintillator readout in PET applications [21–26]. GAPD consists of an array of avalanche photodiode micro-cells operated in Geiger-mode with the output summed from all the microcells, each with an integrated quenching resistor. GAPD has a number of advantages over APD: high gain ($\sim 10^6$), low bias voltage and fast timing response. Since GAPD has higher signal-to-noise ratio (SNR) than APD, electrical noise and EMI shielding requirements are favorable [21]. Additionally, with the advent of tileable GAPD arrays, it is feasible to configure a PET detector having meaningful axial and transaxial FOV. However, still remaining is a characterization of the performance of the scalable GAPD arrays as PET sensor.

The performance of GAPD arrays was measured to investigate its feasibility for MR-compatible PET applications. Primary characteristics of a PET detector, such as energy resolution and coincidence timing resolution were evaluated. Gain variation and count uniformity of 4 $\times$ 4 array of cerium-doped lutetium yttrium orthosilicate (LYSO) coupled to GAPD were measured to evaluate the performance parameters relevant to PET imaging. Count estimation error was measured to test the performance of crystal identification for a PET detector. Photopeak position, energy resolution and count rate as a function of time were measured to examine the long-term stability of the GAPD array. The effect of cable length employed between the GAPD and preamplifier was examined to test the possibility of placing only the crystal-sensor inside the MRI. The performance of the GAPD array was tested in a 7-T MRI scanner to examine the cross compatibility of the LYSO-GAPD array and MRI.

2 Materials and methods

2.1 GAPD array

A 4 $\times$ 4 array of GAPD (SPMArray3035G16, SensL Inc., Ireland) mounted on a 550 μm white float glass substrate using flip chip technology with 16 channel pre-amplification board was employed in this study, as shown in figure 1 (a) [27]. The characteristics of the GAPD are summarized in table 1. Each pixel of the GAPD had a sensitive area of 2.85 mm $\times$ 2.85 mm and a 3.3 mm pitch. The GAPD array was operated at the bias voltage of 29.5 V, exceeding the breakdown voltage by 2.0 V corresponding to a gain of approximately 10^6.

The GAPD signals were preamplified using a 16-channel readout board with high-speed transimpedance amplifiers. The gain of each amplifier was 2200. The 4 $\times$ 4 LYSO (Sinoceramics,

2011 JINST 6 P05012

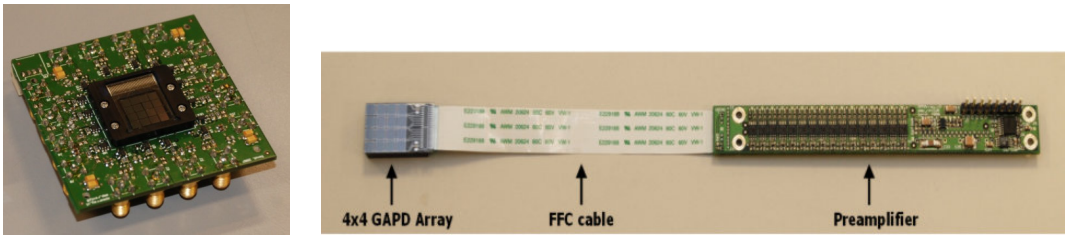

(a) (b)

Figure 1. 4 × 4 array of GAPD mounted on a glass substrate with 16 channel pre-amplification board (a), 4 × 4 array of tilable GAPD on three-sided connected with flexible flat cable (FFC) to preamplifiers with 16 channel differential outputs (b).

Table 1. Specification of 4 × 4 array GAPD.

Pixel chip area	3 mm × 3 mm
Pixel active area	2.85 mm × 2.85 mm
Pixel pitch	3.3 mm
Array details	4 × 4
Glass type	White float glass
Glass thickness	550 μm
Micro cell size	35 μm
Number of individual cells	3640
Quantum Efficiency @ 420 nm	13%
Gain	$\sim \quad 10^6$
Bias voltage	29.5 V
Dark rate	8 MHz

China) array crystal, consisting of 3 mm × 3 mm × 20 mm, was coupled to the GAPD. The crystal blocks had a 12.9 mm × 12.9 mm × 20 mm volume. The individual crystal elements were mechanically polished on all sides and optically isolated with a 0.3 mm white epoxy resin. The LYSO array crystal was coupled to the GAPD array without optical grease.

The GAPD was used for the measurement of energy resolution, timing resolution, gain variation, count uniformity, count estimation error and long-term stability explained in section II. B.

The GAPD array mounted on the preamplifier board shown in figure 1 (a) renders large dead space at the side of the detector. The three-sided tilable GAPD array has been developed to remove the dead space on the threesided and to allow the configuration of a ring type PET detector as shown in figure 1 (b). The three-sided tilable GAPD array was connected to the preamplifier board through flexible flat cable (FFC). The performance and specification characteristics of each pixel are similar to the GAPD array as described in table 1.

2011 JINST 6 P05012

This study was designed to evaluate the basic performance of PET detector using the GAPD array mounted on pre-amplification board. Additionally, the effect of cable length between GAPD and preamplifier and the MR-compatibility were examined using the three-sided tilable GAPD array.

The temperature of the detector modules was stabilized to ambient temperature (20 °C) using a cooling fan and monitored by a microprocessor based digital thermometer during all performance measurements.

2.2 Performance measurements

2.2.1 Energy resolution

The energy spectrum was obtained with a 3.7 μCi ^{22}Na point source. The GAPD was biased with +29.5 V and the preamplifier output was recorded with a multi-channel analyzer. The resulting energy spectra were analyzed to estimate energy resolution. The energy resolution was computed as the full width at half maximum (FWHM) of the 511-keV photopeak.

2.2.2 Timing resolution

The coincidence timing resolution was measured using a pair of PET detectors. Two PET detector modules were located at the opposite sides of each other and separated by 10 mm. A 3.7 μCi ^{22}Na point source was placed in the center of the paired PET detectors. Two channel signals from the two GAPD arrays were sent to 14-bit free-running analog-to-digital converters with a 100 MHz clock (Lyrtech, Canada). The digitized signals were then processed using a field programmable gate array (FPGA) board implemented to calculate the energy and timing information for each gamma ray. The pulse arrival time was obtained by calculating the intersection of the initial rise line with the baseline for each gamma signal pulse [36, 38].

2.2.3 Gain variation and count uniformity

A 3.7 μCi ^{22}Na point source placed 100 mm away from the detector array was used to uniformly irradiate the LYSO array. The 16 channel preamplifier outputs were connected to a custom-made shaping amplifier (figure 2). The outputs of the amplifiers were digitized by peak sensing ADCs. The ADC trigger was generated if one of the 16 channels had a signal above a preset threshold. The energy window for the measurements of the gain variation and the count uniformity was set between 400 and 650 keV. The resulting flood histogram was analyzed in terms of gain variation given by the ratio of highest and lowest photopeak positions and count uniformity given by the ratio of maximum and minimum counts of all 16 channels.

2.2.4 Count estimation error

The count estimation error was estimated by the ratio between counts of the center channel (LYSO coupled) and counts of adjacent channels (without LYSO) using equation as follows:

$$Counts\,estimation\,error = \frac{Counts\,of\,ad\,jacent\,channels}{Counts\,of\,center\,channel\,attached\,with\,a\,LYSO\,pixel} \times 100(\%) \quad (2.1)$$

The count estimation error values for all 16 channels were measured using the experimental setup illustrated set up in figure 3. The influence of the natural activity of the LYSO pixel due to the presence of the ^{176}Lu isotope was not considered.

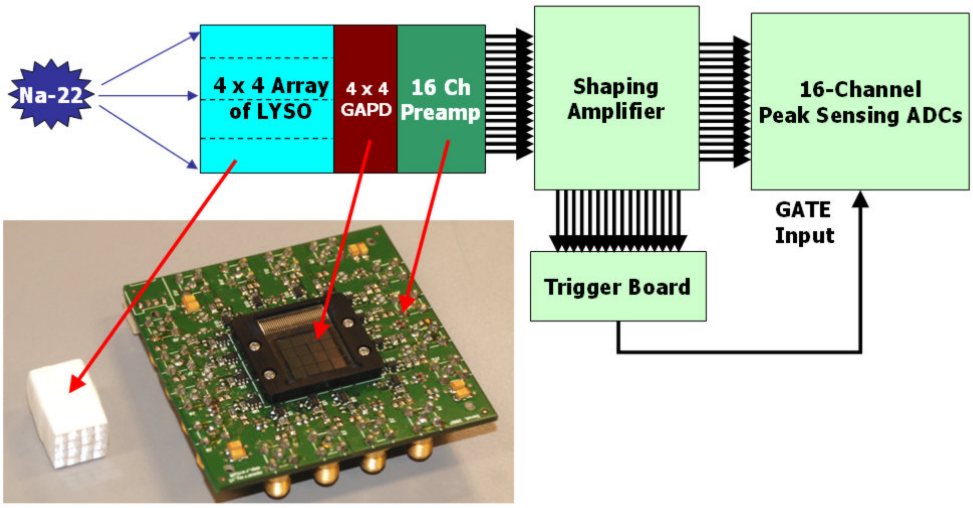

Figure 2. Gain variation and count uniformity measurement setup.

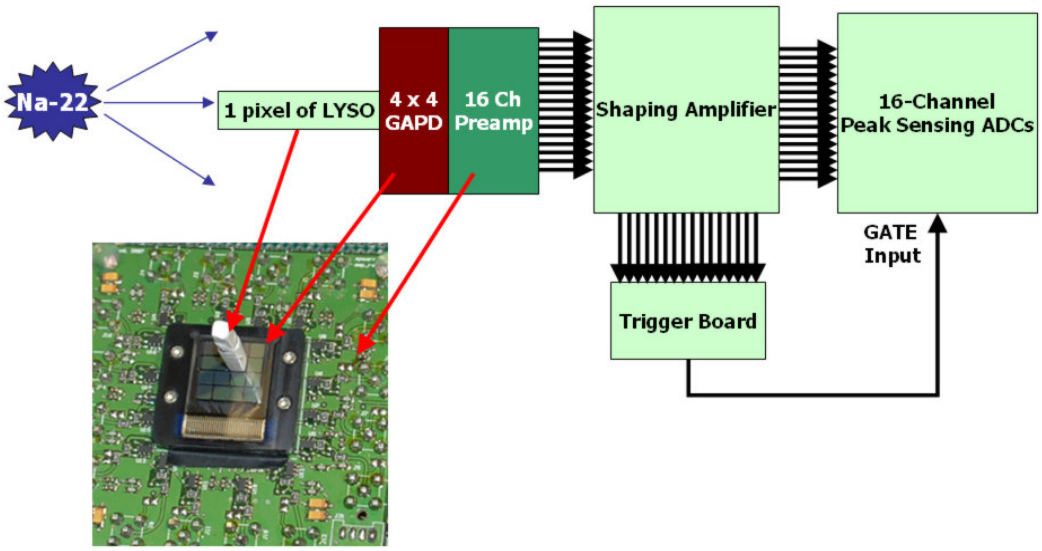

Figure 3. Count estimation error measurement setup.

2.2.5 Long-term stability

A setup identical to the flood histogram experiment was employed. The temperature of the detector module was stabilized at 20 ° and stable bias voltage of +29.5V was supplied during the measurement of the energy spectra. The energy spectra were acquired for 1 hour and the experiment performed for 20 days. The average photopeak position, energy resolution and count rate as a function of day were measured for all 16 channels.

2011 JINST 6 P05012

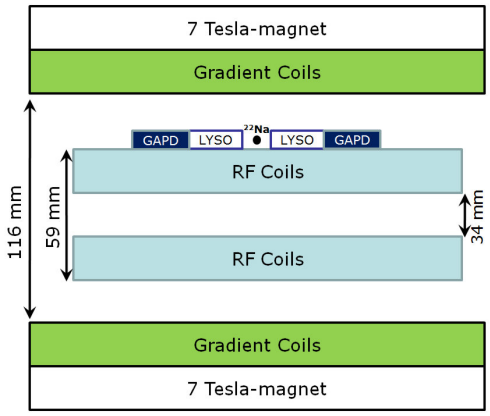

Figure 4. Schematic drawing of the magnet with the gradient coils, PET detectors and RF coils.

2.2.6 Effect of cable length used between GAPD and preamplifier

The three-sided tilable array coupled with a 4 × 4 LYSO crystal array was used in this experiment. Black tape was applied as a shield from light. Flexible flat cable with 39 ways arranged with a pitch of 0.3 mm was used to connect the GAPD output board to a preamplifier board. The length of the cable was varied from 10 cm to 300 cm, with ∼50 cm intervals [37]. For each length of the cable, photopeak channel, energy resolution and timing resolution were measured.

2.2.7 MR-compatibility

As shown in figure 4, the pair of the LYSO-GAPD detectors were inserted inside the MR bore between the RF coil and gradient coils, whereas preamplifiers were positioned outside the MR bore. The experiment was performed on a 7-T animal MRI (Biospec 70/20 USR, Bruker, Germany) using a RF-coil set with a 34 mm inner-diameter/59 mm outer-diameter. The PET detectors were attached to the outside of the RF coil. A black tape was applied to shield the visible light. 300 cm FFC was used to transfer signals from the GAPD to pre-amplifier board positioned outside the MRI. Data were acquired outside and inside the magnet without and with spin echo (SE) T1 sequence (TR = 420 ms, TE = 8 ms, matrix 256×256, pixel size 0.08 mm, 15 transverse slices, slice thickness 1 mm). A data acquisition setup identical to the timing resolution experiment was employed. The power of PET detectors was on when MR images were acquired in the presence of PET detectors.

The evaluation of the signal-to-noise ratio (SNR) and the homogeneity of the MRI obtained with and without the LYSO-GAPD array in the MR imaging FOV, were performed. The two MRI sequences, gradient echo sequence (TR = 206 ms, TE = 6 ms, matrix 256×256, pixel size 0.08 mm, 15 transverse slices, slice thickness 1 mm) and T1-weighted spin echo sequence (TR = 420 ms, TE = 8 ms, matrix 256×256, pixel size 0.08 mm, 15 transverse slices, slice thickness 1 mm) were obtained. A 50 mL tube (inner diameter 10 mm) filled with an aqueous solution containing $CuSO_4$ was used as a homogeneous phantom, placed inside the 34 mm RF coil. The images were analyzed using ImageJ 1.41o (National Institutes of Health, USA). The uniformity of the images was measured by drawing one large (8 mm diameter) region of interest (ROI) on a single MR slice and copying it across all slices containing the phantom. The ROI placement avoided the very edges of

2011 JINST 6 P05012

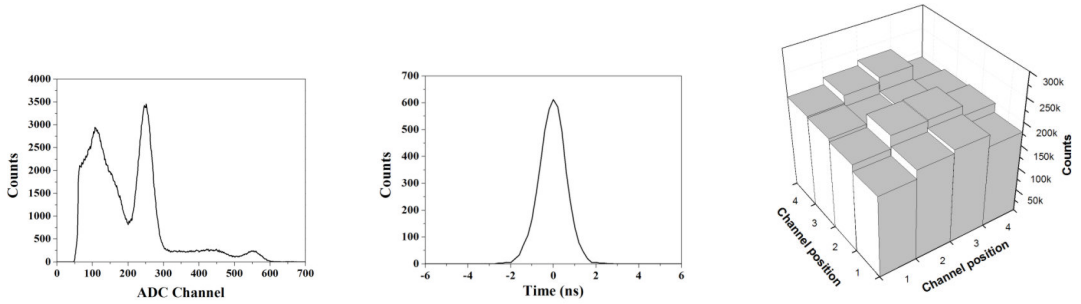

(a) (b) (c)

Figure 5. Energy spectrum (a), timing spectrum (b), and flood histogram (c) acquired with 4 × 4 array of LYSO-GAPD.

Table 2. Performance measurements of the LYSO-GAPD detector.

Energy resolution (n=16)	Timing resolution (n=1)	Gain variation	Count uniformity	Count estimation error (n=16)
18.5 ± 0.7 % FWHM	1.6 ns FWHM	1.3:1	1.3:1	0.24 ± 0.04%

the image where partial-volume effects dominate. The MRI uniformity (%) was defined as follows:

$$MRI\ Uniformity\ (\%) = 100 \times \left(1 - \frac{ROI_{\max} - ROI_{\min}}{ROI_{\max} + ROI_{\min}}\right), \tag{2.2}$$

where ROI_{max} and ROI_{min} are the highest and lowest pixel value in the ROI, respectively [9, 10, 28]. The signal intensity and the noise were estimated by the mean pixel value and the standard deviation of the pixel values, respectively, in an ROI placed centrally on the phantom. The ROI in this case was chosen to be small enough (2 mm diameter) to avoid major contributions from nonuniformity. Uniformity, signal intensity, and noise were compared across imaging conditions, with and without the LYSO-GAPD array present.

3 Results

3.1 Performance of the GAPD array

The performance measurements of the LYSO-GAPD detector are summarized in table 2. Figure 5 (a, b) shows a representative energy and timing spectrum from a ^{22}Na source, acquired with the LYSO-GAPD detector. The energy resolution and count estimation error were measured for all 16 channels (n=16). The timing resolution was measured for one channel (n=1). The flood histogram of data acquired with 4 × 4 array of LYSO-GAPD is shown in figure 5 (c).

The results of this study demonstrate that the LYSO-GAPD detector can provide a good energy resolution, timing resolution, gain variation, count uniformity and count estimation error for a PET detector.

2011 JINST 6 P05012

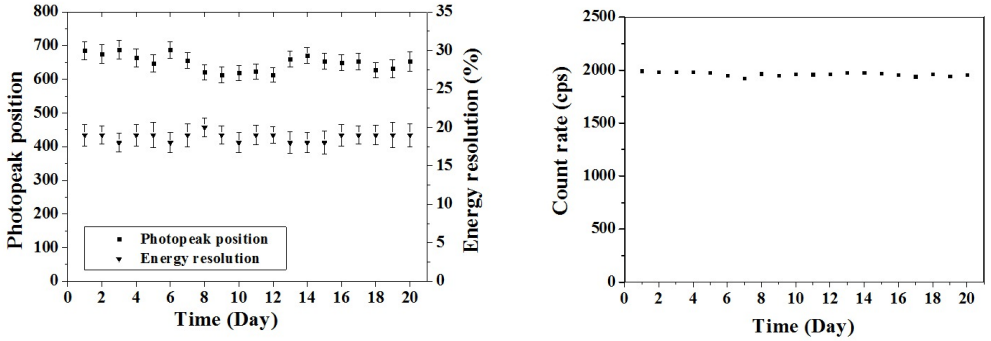

(a) (b)

Figure 6. The average photopeak position, average energy resolution (a) and count rate (b) as a function of day. The error bar is the standard deviation of 16 channels.

3.2 Long-term stability

Figure 6 shows the average photopeak position, average energy resolution and count rate for 20 days. The average photopeak and average energy resolution were measured for all 16 channels (n=16). The count rate was measured as the total counts for all 16 channels. The average photopeak position, average energy resolution and average count rate were 649.5 $\pm$ 24.7 ADC channel, 18.7 $\pm$ 0.4% and 1962 $\pm$ 16.9 cps, respectively, where the data were represented as mean $\pm$ standard deviation (sigma) measured for 20 days. The coefficients of variation (standard deviation/mean) for the three factors above were 3.8%, 2.1% and 0.9%, respectively. Long-term stability results show that there was no significant change in the photopeak position, energy resolution and count rate for 20 days.

3.3 Effect of cable length used between GAPD and preamplifier

Figure 7 shows the effect of cable length used between GAPD and preamplifier on 511-keV photopeak position, energy resolution and timing resolution. The three factors were measured for one channel (n=1). The maximum change of the photopeak channel, energy resolution and timing resolution compared to the values acquired with 10 cm cable were 7.6%, 2.5% and 17.6%, respectively. The coefficients of variation for the three factors above were 2.2%, 1.1% and 6.1%, respectively.

The cable length up to 300 cm used between GAPD and preamplifier did not considerably affect photopeak position and energy resolution. This result indicates the possibility of placing only the crystal-sensor inside the MRI and subsequent electronics outside the fringe magnetic field.

3.4 MR-compatibility

The energy resolution, timing resolution and 511-keV photopeak position with the LYSO-GAPD array outside and inside the MRI with and without SE T1 sequence are summarized in table 3.

The results when the detector was located inside the MRI and while SE T1 sequence was being performed showed no significant changes compared with the results acquired outside the MRI.

SE and GE sequences were run in the presence of the PET module in the MR imaging FOV. No obvious artifacts can be observed in the resulting phantom images when compared with the

2011 JINST 6 P05012

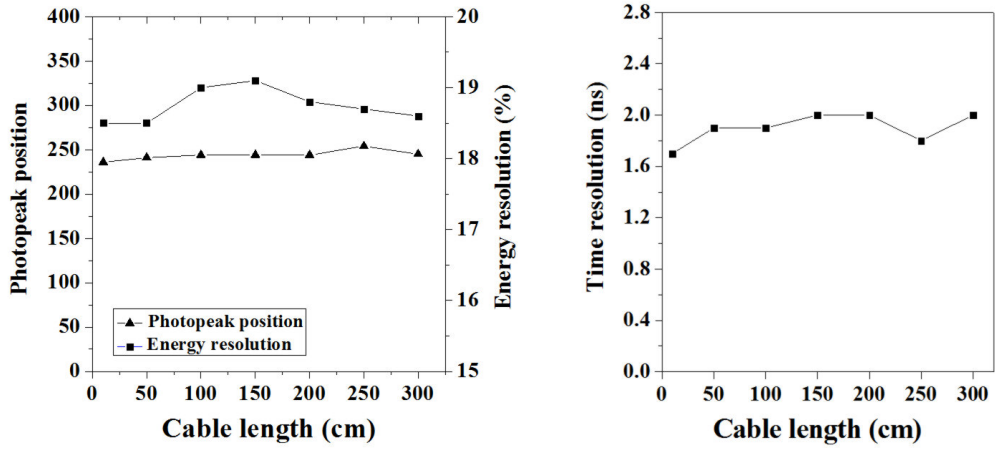

(a) (b)

Figure 7. Photopeak channel, energy resolution (a) and timing resolution (b) as a function of various cable lengths.

Table 3. Energy resolution and timing resolution measured with the LYSO-GAPD array inside and outside the MRI scanner.

	Outside MRI	Inside 7T	Inside 7T with SE T1
Energy Resolution (% FWHM)	18.6	18.4	18.0
Timing Resolution (ns FWHM)	1.6	1.5	1.7
511-keV photopeak position (ADC channel)	245	249	251

ones acquired without the PET module (figure 8). The signal intensity, noise, and uniformity of the MR images under the different imaging conditions are shown in table 4. The data confirm the visual evidence that there was no obvious degradation in the MRI performance in the presence of the PET module in MRI FOV when standard MR pulse sequences were employed.

4 Discussion and conclusion

The basic performance of a PET detector made of an LYSO array coupled to a 4 ×g array of large-size GAPD was investigated in this study. The energy resolution for 511 keV photopeak and timing resolution was 18.5% and 1.6 ns, respectively. These results are similar to those obtained recently by other authors using the same GAPD array used in this study. Olcott et al. employed a single 3 mmg× 3 mmg× 20 mm LYSO crystal coupled to the GAPD array [29] and obtained 15.5%

2011 JINST 6 P05012

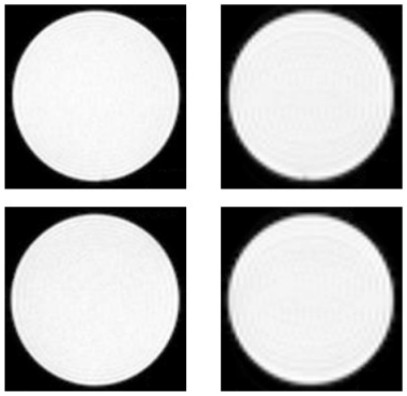

(a) (b)

Figure 8. MR phantom images acquired without (top row) and with (bottom row) the PET detector module inside MR imaging FOV. MR phantom images were acquired with gradient (a) and spin (b) echo sequences.

Table 4. Effect of PET module on MR phantom images.

	GE		SE	
Parameter	Without PET module	With PET module	Without PET module	With PET module
Signal	247.9	247.3	241.5	239.1
Noise	1.8	1.7	0.9	0.9
Signal-to-noise ratio	1377	145.5	2683	2657
Uniformity (%)	95.0	94.6	95.3	94.6

Units: pixel value.

energy resolution and 1.3 ns timing resolution. Schaart et al. reported 14.2% energy resolution and 1.4 ns timing resolution using a 13.2 mm $\times$ 13.2 mm $\times$ 10 mm monolithic LYSO crystal coupled to the GAPD array [39]. The slight difference in the results could be attributed to the different experimental setting for example, using a PMT as a coincidence detector in the previous study.

The energy and timing resolution of the GAPD array with the preamplifier board (figure 1 (a)) and of the three-sided tilable GAPD array (figure 1 (b)) showed similar results. For example, the energy resolutions of the both types GAPD array were 18.5 % (table 2) and 18.6% (table 3, outside MRI), respectively. The timing resolution of the both types GAPD array were 1.6 ns (table 2) and 1.6 ns (table 3, outside MRI), respectively. The results indicated that the performance of both types GAPD arrays was similar because both of the GAPD arrays were fabricated with the same type of Geiger-mode avalanche photodiode micro-cells.

Although the experimental measurements of this work were conducted with commercially available electronics which were not optimized for reading the GAPD arrays, the results still demonstrate the feasibility of using the GAPD arrays to replace PMT in a PET detector. The mean energy resolution of the LYSO-GAPD detector obtained in this study was comparable to the value

2011 JINST 6 P05012

(18.5 $\pm$ 0.7 %) of commercial PET employing LSO-PMT [30, 31]. The timing resolution of the LYSO-GAPD detector, 1.6 ns obtained in this study was also similar to that (2 ns) of a LSO-PMT based system [32].

Gain of each channel in multi-channel photosensor was commonly non-uniform, for example, the gain variation of PMT was typically 3:1 [33, 34]. The LYSO-GAPD array used in this study demonstrated better gain variation (1.3:1) than that of LSO-PMT, partly because optical binning techniques were used at wafer level to allow GAPD array with uniform pixel responses to be assembled with $<$10% variation (defined as the standard deviation/mean of all 16 pixels in the GAPD array). The small gain variation was related to the good count uniformity (1.3:1) in the uniform source images.

The count estimation error of LYSO-GAPD detector measurement was studied to test the inter-channel count estimation error of the GAPD for correctly identifying the crystal of interaction for a gamma ray imaging detector. The count estimation error of LYSO-GAPD detector between adjacent channels measured with a LYSO connected to a GAPD pixel was less than 0.3% which was superior to that of the multi-anode type photomultiplier tube (3%) [35].

The long-term stability results showed the possibility of that the sensor could be employed to construct a PET system requiring a stable performance over time, although a longer term stability study is necessary. The slight variations of the photopeak position and energy resolution could be partly attributed to the temperature fluctuation of an air conditioner used for stabilizing the temperature of the detector module. Nevertheless, the average photopeak position and average energy resolution showed small variations of 7% and 2%, respectively. Additionally, the variation of the count rate was 1% which indicated that the detector could provide consistent count rate over time. If the temperature of the detector module could be adjusted precisely, using a cooling chamber, the stability of the detector module would be improved.

The effect of cable length used between the GAPD and preamplifier evaluated in this study demonstrated that there was no decrease in the performance of the detector module, even if 3-meter cable was used between the GAPD and preamplifier. This cabling method will make it easier to build an insertable PET capable of working within the bore of a conventional MR, while leaving most of the associated electronics in a separate location with lower magnetic flux density next to the MR gantry. Also, when this cable is used with the MR system, the heat generated in front-end electronics does not affect the sensor directly, so then there is no degrading effect on sensor performance.

The results of MR-compatibility test demonstrated that simultaneous high-field-strength MR and PET imaging is feasible and the overall performance of each modality is preserved. The PET detector did not affect the operation of the MR imaging system, and likewise, the PET detector performance was not compromised during MR imaging. The MR phantom images showed no visible artifact when imaging was performed while operating PET a detector located on top of the RF coil. The signal-to-noise ratios and uniformity confirmed the visual evidence that there was no obvious degradation with or without PET detector materials inside the MR imager. However, potential artifacts from a full-ring PET system, requiring far more PET detectors and electronics in the magnet need to be evaluated further to show whether MR image quality is maintained.

These results demonstrate the feasibility of using a PET detector consisting of an LYSO array coupled to a 4 $\times$ 4 array of large-size GAPD comparable to the current PMT-based PET detec-

2011 JINST 6 P05012

tors. In addition, the LYSO-GAPD array can provide the consistent long-term stability, the MR-compatibility and the possibility of using a long cable ($\sim$ 300 cm) from the GAPD to preamplifier.

Acknowledgments

This study was supported by a grant of the Converging Research Center Program through the National Research Foundation of Korea (NRF) funded by the Ministry of Education, Science and Technology (2010K001109), and by a grant of the Technology Innovation Program funded by, the Ministry of Knowledge Economy (10030029), Republic of Korea.

References

[1] D.W. Townsend et al., *PET/CT today and tomorrow*, *J. Nucl. Med.* **45 1** (2004) 4S.

[2] G. Antoch et al., *Accuracy of whole-body dual-modality Fluorine-182-fluoro-2-Deoxy-D-Glucose Positron Emission Tomography and Computed Tomography (FDG-PET/CT) for tumor staging in solid tumors: comparison with CT and PET*, *J. Clin. Oncol.* **22** (2004) 4357.

[3] T. Beyer et al., *Acquisition protocol considerations for combined PET/CT imaging*, *J. Nucl. Med.* **45** Suppl. **1** (2004) 25S.

[4] P. Marzola et al., *High field MRI in preclinical research*, *Eur. J. Radiol.* **48** (2003) 165.

[5] M.S. Judenhofer et al., *Simultaneous PET-MRI: a new approach for functional and morphological imaging*, *Nature Med.* **14** (2008) 459.

[6] B.J. Pichler et al., *Positron Emission Tomography/Magnetic Resonance imaging: the next generation of multimodality imaging?*, *Sem. Nucl. Med.* **38** (2008) 199.

[7] M.S. Judenhofer et al., *PET/MR images acquired with a compact MR-compatible PET detector in a 7-T magnet*, *Radiology* **244** (2007) 807.

[8] R.R. Raylman et al., *Simultaneous acquisition of magnetic resonance spectroscopy (MRS) data and positron emission tomography (PET) images with a prototype MR-compatible, small animal PET imager*, *J. Magn. Resonance* **186** (2007) 305.

[9] C. Catana et al., *Simultaneous acquisition of multislice PET and MR images: initial results with a MR-compatible PET scanner*, *J. Nucl. Med.* **47** (2006) 1968.

[10] B.J. Pichler et al., *Performance test of an LSO-APD detector in a 7-T MRI scanner for simultaneous PET/MRI*, *J. Nucl. Med.* **47** (2006) 639.

[11] R.R. Raylman et al., *Simultaneous MRI and PET imaging of a rat brain*, *Phys. Med. Biol.* **51** (2006) 6371.

[12] Y. Shao et al., *Development of a PET detector system compatible with MRI/NMR systems*, *IEEE Trans. Nucl. Sci.* **44** (1997) 1167.

[13] Y. Shao et al., *Simultaneous PET and MR imaging*, *Phys. Med. Biol.* **42** (1997) 1965.

[14] R. Slates et al., *Design of a small animal MR compatible PET scanner*, *IEEE Trans. Nucl. Sci.* **46** (1999) 565.

[15] S. Yamamoto et al., *A block detector for a multislice, depth-of-interaction MR-compatible PET*, *IEEE Trans. Nucl. Sci.* **52** (2005) 33.

2011 JINST 6 P05012

[16] R. Lecomte et al., *Initial results from the Sherbrooke avalanche photodiode positron tomograph*, *IEEE Trans. Nucl. Sci.* **43** (1996) 1952.

[17] Y. Yang et al., *Depth of interaction resolution measurements for a high resolution PET detector using position sensitive avalanche photodiodes*, *Phys. Med. Biol.* **51** (2006) 2131.

[18] S.I. Ziegler et al., *A prototype high-resolution animal positron tomograph with avalanche photodiode arrays and LSO crystals*, *Eur. J. Nucl. Med.* **28** (2001) 136.

[19] B. Pichler et al., *Studies with a prototype high resolution PET scanner based on LSO-APD modules*, *IEEE Trans. Nucl. Sci.* **45** (1998) 1298.

[20] T.Y. Song et al., *Characterization of two deep-diffusion avalanche photodiode array prototypes with different optical coatings*, *IEEE Trans. Nucl. Sci.* **51** (2004) 2279.

[21] V.C. Spanoudaki et al., *Use of single photon counting detector arrays in combined PET/MR: characterization of LYSO-SiPM detector modules and comparison with a LSO-APD detector*, 2007 *JINST* **2** P12002.

[22] V.D. Kovaltchouk et al., *Comparison of a silicon photomultiplier to a traditional vacuum photomultiplier*, *Nucl. Instrum. Meth.* **A 538** (2005) 408.

[23] D.J. Herbert et al., *First results of scintillator readout with silicon photomultiplier*, *IEEE Trans. Nucl. Sci.* **53** (2006) 389.

[24] D. Renker, *Geiger-mode avalanche photodiodes, history, properties and problems*, *Nucl. Instrum. Meth.* **A 567** (2006) 48.

[25] Y. Shao et al., *Initial experimental studies of using solid-state photomultiplier for PET applications*, *Nucl. Instrum. Meth.* **A 580** (2007) 944.

[26] A.N. Otte et al., *A test of silicon photomultipliers as readout for PET*, *Nucl. Instrum. Meth.* **A 545** (2005) 705.

[27] P.J. Hughes et al., *Tiled silicon photomultipliers for large-area low-light sensing applications*, *Proc. SPIE Int. Soc. Opt. Eng.* **6471** (2007) 647112.

[28] R.R. Price et al., *Quality assurance methods and phantoms for magnetic resonance imaging: report of AAPM nuclear magnetic resonance task group no.* 1, *Med. Phys.* **17** (1990) 287.

[29] P.D. Olcott et al., *Novel electro-optical coupling technique for magnetic resonance-compatible positron emission tomography detectors*, *Mol. Imaging* **8** (2009) 74.

[30] Y.C. Tai et al., *Performance evaluation of the microPET focus: a third-generation microPET scanner dedicated to animal imaging*, *J. Nucl. Med.* **46** (2005) 455.

[31] S. Yamamoto et al., *Investigation of single, random, and true counts from natural radioactivity in LSO-based clinical PET*, *Ann. Nucl. Med.* **19** (2005) 109.

[32] K. Ziemons et al., *The ClearPET™ project: development of a* 2nd *generation high-performance small animal PET scanner*, *Nucl. Instrum. Meth.* **A 537** (2005) 307.

[33] Y.P. Shao et al., *Evaluation of multi-channel PMTs for readout of scintillator arrays*, *Nucl. Instrum. Meth.* **A 390** (1997) 209.

[34] M. Streun et al., *Effects of crosstalk and gain nonuniformity using multichannel PMTs in the ClearPET® scanner*, *Nucl. Instrum. Meth.* **A 537** (2005) 402.

[35] Datasheet Hamamatsu, *Multianode photomultiplier tube H*8500, Hamamatsu Photonics K. K., Electron Tube Center, 314-5, Shimokanzo, Japan.

2011 JINST 6 P05012

[36] W. Hu et al., *A simple and improved digital timing method for Positron Emission Tomography*, *Nucl. Instrum. Meth.* **A 622** (2010) 219.

[37] J. Kang et al., *A feasibility study of photosensor charge signal transmission to preamplifier using long cable for development of hybrid PET-MRI*, *Med. Phys.* **37** (2010) 5655.

[38] J.H. Jung et al., *Development of a position decoder circuit for PET consisting of GAPD arrays*, *Nucl. Instrum. Meth.* **A 621** (2010) 310.

[39] D.R. Schaart et al., *A novel, SiPM-array-based, monolithic scintillator detector for PET*, *Phys. Med. Biol.* **54** (2009) 3501.

2011 JINST 6 P05012